International Journal of Heat and Mass Transfer 82 (2015) 545–554

Contents lists available at ScienceDirect

International Journal of Heat and Mass Transfer

journal homepage: www.elsevier.com/locate/ijhmt

Optical and thermal radiative properties of plasmonic nanofluids containing core–shell composite nanoparticles for efficient photothermal conversion

Ya Wu, Leping Zhou *, Xiaoze Du *, Yongping Yang

School of Energy, Power and Mechanical Engineering, Key Laboratory of Condition Monitoring and Control for Power Plant Equipment of Ministry of Education, North China Electric Power University, Beijing 102206, China

ARTICLE INFO

Article history:
Received 1 August 2014
Received in revised form 21 October 2014
Accepted 8 November 2014
Available online 26 November 2014

Keywords:
Core–shell structure
Localized surface plasmon resonance
Extinction coefficient
Near field radiation

ABSTRACT

Nanofluid has been proposed for use in direct absorption solar collector because of its unique thermal and optical radiative properties. The improvement of solar absorption efficiency was shown to be significantly influenced by the particle material, size, shape, volume fraction, etc. However, it was rare for simultaneously investigating the thermal and optical properties, especially the spectral ones that are critical for efficient photothermal application. Nonmetallic nanoparticles with metallic nanoshells can improve the spectral solar absorption efficiency since the effect of localized surface plasmon resonance (LSPR) exists at the surfaces of these core–shell composite nanoparticles. In this paper, the effect of LSPR at the surfaces of some typical composite nanoparticles (with Si or SiC core and Au, Ag, Cu or Al shell) on the optical and thermal radiative properties of water-based plasmonic nanofluids is numerically investigated by varying the particle radius ratio, outer radius and type of material of the composite nanoparticles in the dependent scattering regime through setting the volume fraction or particle distance. The scattering, absorption or extinction coefficient for these nanoparticles are calculated using the Mie scattering theory and the Rayleigh scattering approximation. The order of magnitude of near field interactions between the nanoparticles is demonstrated by two parallel nanoparticle arrays, based on the near field radiation heat flux between two nanoparticles using the fluctuation electrodynamics. The contributions of the optical absorption and thermal radiation in the near field are compared with the effective thermal conductivity of the nanofluids. The results show that the structure itself can simultaneously influence the average and the near field radiative properties of the composite nanoparticles and thus the plasmonic nanofluids. These coupling effects can be efficiently utilized for tuning the radiative properties of plasmonic nanofluids used in photothermal application.

1. Introduction

Optical and thermal radiative properties of advanced materials are critically needed for solar energy conversion systems, photothermal management, etc. Nanofluid has been proposed for use in direct absorption solar collector because of its unique thermal and optical properties [1] since it was first reported with abnormally high thermal conductivity [2]. For example, Yousefi et al. [3] experimentally investigated the effect of Al_2O_3/H_2O nanofluid on the efficiency of flat-plate solar collectors. Their results show an increased efficiency of 28.3% comparing with water when the mass concentration is 0.2%. Tyagi et al. [4] theoretically studied the capability of using nanofluid in non-concentrating direct absorption solar collector and found that its efficiency is up to 10% higher than that used in a flat-plate collector. Otanicar et al. [1] experimentally studied the effect of different nanofluids used in solar thermal collectors and obtained an efficiency improvement up to 5%. The efficiency improvements were shown to be significantly influenced by the particle material, size, shape, volume fraction, etc [5]. However, it was rare in the literature for simultaneously investigating the thermal and optical properties, especially the spectral ones.

The research on the scattering and absorption characteristics of a simple particle with diameter smaller than the radiation wavelength can be traced back to the works by Rayleigh and later Lorenz, Mie, Debye, et al. More details about the history of scattering can be referred to, e.g., Modest's book [6]. Recently, with the

* Corresponding authors. Tel.: +86 10 61773873.
E-mail address: lpzhou@ncepu.edu.cn (L. Zhou).

http://dx.doi.org/10.1016/j.ijheatmasstransfer.2014.11.026
0017-9310/

Nomenclature

a	particle radius (m)
c	speed of light (m/s)
C	cross-section (m^2)
d	center-to-center distance (m)
D	diameter (m)
f	volume ratio
f_v	volume fraction
F	form factor
g	pair distribution function
$\boldsymbol{G}$	Green's function
h	Planck constant (J s)
$\hbar$	reduced Planck constant (J s)
k_B	Boltzmann constant (J/K)
k_{eff}	effective thermal conductivity (W/(m K))
k_r	average radiative thermal conductivity (W/(m K))
k_{nf}	average near field radiative thermal conductivity (W/(m K))
K	optical constant
n	refractive index
N_T	particle number in unit volume
P	radiation heat transfer power volume ratio
Pr	Prandtl number
Q	scattering efficiency mean energy of an oscillator (J)
r	radius (m) distance from the central scatterer (m)
R_λ	blackbody radiation intensity (J/(m Hz))
s	radiation heat transfer area (m^2)
S	Poynting vector, near field radiation heat flux (W/m^2)
t	radius ratio
T	temperature (°C)
x	non-dimensional size parameter

Greek symbols

α	polarizability, polarization
ε	dielectric function
Φ	phase function
Γ	scattering rate
λ	wavelength (m)
Θ	angle between directions of propagation and observation (rad)
σ	extinction coefficient Stefan Boltzmann constant (J/(s m^2 K^4))
ω	frequency (rad/s)
Ω	solid angle (sr)

Subscripts

0	vacuum
1	core
2	shell
∞	high frequency contribution
a,abs	absorption
bf	base fluid
cr	critical
ext	extinction
p	nanoparticle plasma
s,sca	scattering

Superscripts

e	perpendicular polarization
m	parallel polarization
M	Mie scattering
SD	dependent scattering
SM	Mie scattering
TE	perpendicular polarization
TM	parallel polarization

development of nanoparticle (NP) and its potential application in fluids for solar energy conversion, the radiative properties of nanoparticles including the absorption and scattering coefficients and the induced extinction coefficient were attracting much attention [7]. For example, the optical properties of metallodielectric nanostructures, such as the optical absorption and scattering cross sections as well as the local electromagnetic fields and induced charge densities at the surfaces of the nanostructures, can be obtained by the finite difference time domain (FDTD) method [8,9]. The material and the shape of nanoparticle are two important factors influencing the spectral properties of fluids. An effective method for obtaining the spectral properties of fluids is by using and controlling the core–shell composite nanoparticles [10,11]. Core–shell composite nanoparticle can be prepared by many chemical reaction method [12–15]; however, the absorption and scattering characteristics of these novel nanoparticles need to be verified.

Three scattering regimes can be defined using the non-dimensional size parameter $x = \pi D/\lambda$ where D is the nanoparticle diameter and λ is the wavelength of the incident radiation: Rayleigh scattering ($x \ll 1$), Mie scattering ($x = 1$), and geometric scattering ($x \gg 1$) [16]. When nanoparticle size is close to the wavelength, the coupling effects between particles including multiple interference, near field radiation or the surface plasma should be considered. For instance, Volz et al. [17] investigated the near-filed radiative heat transfer in nanoparticle based composite media and obtained the effective thermal conductivity due to the near field radiation. Lu et al. [18] developed the three critical point pole pairs (CP3) model to better describe the dielectric functions for the dispersions of metal nanoparticles and used the FDTD method to study the effect of the interaction between the SiO_2/Au core–shell composite nanocylinder pair on the localized surface plasmon resonance (LSPR) spectra. Phan et al. [19] studied the near field heat transfer between gold nanoparticle arrays using the coupled dipole method and found that the near field radiation reduces with increasing nanoparticle size. These investigations show that details about the effect of the material and the size of nanoparticle needs for further discussion.

In this paper, we will investigate the optical and thermal radiative properties of water-based plasmonic nanofluids containing core–shell composite nanoparticles through absorption, extinction and near filed radiation heat transfer in the nanoparticles at wavelength scale by changing the material, size, structure and volume fraction, in order to vary the spectral absorption properties of these nanofluids that could be used in direct absorption solar collector.

2. Theory

2.1. Absorption and extinction

The optical radiative properties involving light absorption and scattering in a media is related to the extinction effect. During the absorption and scattering processes, surface plasmon resonance (SPR) plays an important role that influence the extinction coefficient. SPR is the collective oscillation of surface electrons

illuminated by incident light if the frequency of light photons matches the natural frequency of electrons oscillating against the restoring force of positive nuclei. For metallic nanoparticles or nanostructures, LSPR that is responsible for the sharp spectral absorption and scattering peaks as well as strong electromagnetic near field enhancement can be created if the size is smaller than the incident wavelength [20]. This effect can be utilized by controlling the shape and the size of nanoparticle and thus tuning the resonance wavelength and intensity for harvesting solar energy such as solar thermal collectors and solar cells [21]. Plasmonic fluids containing nanoparticles with different metallic shells that are expected to have the excited LSPR effect were therefore proposed for efficient spectral solar absorption [11]. LSPR excitation in these core–shell composite nanoparticles could produce strong extinction and scattering spectra that can be many orders of magnitude larger than without LSPR [22]. We will therefore investigate the LSPR effect on different core–shell composite nanoparticles in the following.

For plasmonic fluid containing core–shell composite nanoparticles, the extinction effect includes the contribution of both the nanoparticles and the base fluid. From the definition of scattering regimes for nanoparticles [16], the dependent scattering effect can be neglected when the volume fraction $f_v < 0.6\%$ or $d/\lambda > 0.5$, where d is the center-to-center distance between two nanoparticles, $f_v = (4\pi/3)(D/(2d))^3$ and d/λ is the distance wavelength ratio. When the particles are in the dependent region, d/λ will be replaced by d/a, where a is the radius. So here we fix the nanoparticle volume fraction to $f_v = 0.7\%$ to study the dependent scattering effect for $d/\lambda < 0.5$ by Rayleigh scattering theory [23]. For nanoparticle with diameter larger than 10 nm, the LSPR effect has been studied extensively. However, for nanoparticle with diameter smaller than 10 nm, which has been successfully synthesized in the experiments [24], the light scattering and reflection are weaker and the nanoparticle will have the metal ligand effect (aggregation effect) [25], presenting a potential way for enhancing the heat transfer. So we fix the nanoparticle diameter to $D = 10$ nm.

Assuming that the medium is continuous, isotropy, well-distributed and infinity, the scattering, absorption or total extinction coefficient ($\sigma_{s,\lambda}$, $\sigma_{a,\lambda}$ or $\sigma_{ext,\lambda}$) for nanoparticles can be calculated by the product of scattering, absorption or extinction cross-section (C_{sca}, C_{abs} or C_{ext}) and the particle number in unit volume ($N_T = 6f_v/(\pi D^3)$) using the Mie scattering theory (which neglects higher order terms) and the Rayleigh scattering approximation [4,6]. The ratio of the scattering or absorption cross-section to πa^2 are defined as the scattering or absorption efficiency (Q_{sca} or Q_{abs}) of particles, while the ratio of the extinction cross-section to πa^2 is the sum of the scattering and absorption efficiencies ($Q_{ext} = Q_{sca} + Q_{abs} = C_{ext}/(\pi a^2)$). For pure metal nanoparticles, the scattering and absorption efficiencies are [23]

$$Q_{sca} = \frac{8}{3}x^4\left|\frac{m^2-1}{m^2+2}\right|^2 \tag{1}$$

$$Q_{abs} = 4x\left\{\frac{m^2-1}{m^2+2}\left[1+\frac{a^2}{15}\left(\frac{m^2-1}{m^2+2}\right)\frac{m^4+27m^2+38}{2m^2+3}\right]\right\} \tag{2}$$

respectively, where $m = n_p/n_{bf}$ is the relative refractive index between nanoparticle and base fluid. While for core–shell composite nanoparticles, the absorption and scattering efficiencies can be obtained by using the quasi-static approximation of the dipole model [11,26]

$$\begin{aligned} Q_{sca} &= C_{sca}/(\pi a^2) = \frac{k^4}{6\pi}|\alpha|^2/(\pi a^2) \\ &= \frac{128\pi^5}{3\lambda^4}\varepsilon_3^2 r_2^6\left|\frac{\varepsilon_2\varepsilon_\alpha-\varepsilon_3\varepsilon_b}{\varepsilon_2\varepsilon_\alpha+2\varepsilon_3\varepsilon_b}\right|^2\Big/(\pi a^2) \end{aligned} \tag{3}$$

$$\begin{aligned} Q_{abs} &= C_{abs}/(\pi a^2) = k\,\mathrm{Im}(\alpha)/(\pi a^2) \\ &= \frac{8\pi^2\sqrt{\varepsilon_3}}{\lambda}r_2^3\,\mathrm{Im}\left(\frac{\varepsilon_2\varepsilon_\alpha-\varepsilon_3\varepsilon_b}{\varepsilon_2\varepsilon_\alpha+2\varepsilon_3\varepsilon_b}\right)\Big/(\pi a^2) \end{aligned} \tag{4}$$

with the polarizability $\alpha = 4\pi r_2^3[(\varepsilon_2\varepsilon_a - \varepsilon_3\varepsilon_b)/(\varepsilon_2\varepsilon_a + 2\varepsilon_3\varepsilon_b)]$, where $k = 2\pi/\lambda n_p$, r_1 and r_2 are the radius of core and shell, respectively, ε_1 and ε_2 are the dielectric functions of core and shell, respectively, and ε_a and ε_b are the effective dielectric functions:

$$\varepsilon_a = \varepsilon_1(3-2P) + 2\varepsilon_2 P \tag{5}$$

$$\varepsilon_b = \varepsilon_1 P + \varepsilon_2(3-P) \tag{6}$$

where $P = 1 - (r_1/r_2)^3$ is the ratio of the shell volume to the total particle volume. The ratio of the absorption efficiency (Q_{abs}) to the total efficiency ($Q_{abs} + Q_{sca}$) is defined as the overall acceptance.

For both pure metal and core–shell composite nanoparticles, the scattering, absorption and total extinction coefficients are

$$\sigma_{s,\lambda} = C_{sca}N_T = \pi a^2 Q_{sca}N_T \tag{7}$$

$$\sigma_{a,\lambda} = C_{abs}N_T = \pi a^2 Q_{abs}N_T \tag{8}$$

$$\sigma_{ext,\lambda} = \sigma_{s,\lambda} + \sigma_{a,\lambda} = C_{ext}N_T = \pi a^2 Q_{ext}N_T \tag{9}$$

respectively. The extinction coefficient of base fluid and hence the total extinction coefficient of nanofluid can be obtained from Eqs. (10) and (11), respectively.

$$\sigma_{bf,\lambda} = 4\pi K_{bf}/\lambda \tag{10}$$

$$\sigma_{tot,\lambda} = \sigma_{bf,\lambda} + \sigma_{ext,\lambda} \tag{11}$$

Here K_{bf} is the optical constant of water [23,27].

The dependent scattering efficiency can be calculated via the form factor technique based on the X-ray scattering theory [25]. This technique uses a pair distribution function $g(r)$ that represents the probability of finding a neighboring sphere at a distance r from some central spheres to correlate the relative positions of the constituent particles in the system. Here the Percus–Yevick (PY) pair distribution function for the hard-sphere potential [28], which means that the hemispherical reflectance is independent of the thickness of the composite layer and thus is not due to multiple scattering, is employed. Then the interference effects can be quantified by the dependent scattering models that follow the form factor $F(\Theta)$ approach from X-ray scattering theory:

$$F(\Theta) = 1 + 24f_v\int_0^\infty r^{*2}[g(r^*)-1]\frac{\sin(Sr^*)}{Sr^*}\mathrm{d}r^* \tag{12}$$

where $r^* = r/D$, $S = 4x\sin(\Theta/2)$, r is the distance from the central scatterer, and Θ is the angle between directions of propagation and observation. The dependent scattering efficiency Q_{SD} for a given particle is thus calculated by

$$Q_{SD}/Q_{SM} = \frac{1}{4\pi}\int_{4\pi} F(\Theta)\Phi_M(\Theta)d\Omega \tag{13}$$

where Q_{SM} is the Mie scattering extinction efficiency, $\Phi_M(\Theta)$ is the Mie scattering phase function, and Ω is the solid angle. The PY integral equation with the appropriate potential function for particle–particle interactions approaches the "gas" model at low f_v (<0.1), which means no neighbor exists within one particle diameter of the central scatter and the likelihood of finding a neighbor outside this diameter is uniform. Therefore $g(r^*) = 0$ for $r^* < 1$ and $g(r^*) = 1$ for $r^* > 1$. Then $F(\Theta)$ reduces to $(1-fv)^4/(1+2fv)^2$ and thus the reduced scattering efficiency is $Q_{SD}/Q_{SM} = (1-fv)^4/(1+2fv)^2$ when $x \to 0$. Since f_v is set to be 0.7%, $Q_{SD}/Q_{SM} = 0.9456$. This indicates that the ratio of dependent scattering efficiency and Mie scattering extinction efficiency is dependent on the volume fraction and is a constant. Hence we simply calculate the spectral characteristics for different core–shell composite nanoparticles with consideration only of the Mie scattering extinction efficiency.

2.2. Dielectric function

Before calculation of the extinction coefficient using the above-mentioned equations, one needs to decide the dielectric functions of the composites, i.e., core and metal shells. The dielectric function of metal can be obtained by the Drude model [29]

$$\varepsilon(\omega) = \varepsilon_\infty - \frac{\omega_p^2}{\omega^2 + i\omega\Gamma} \tag{14}$$

where ε_∞ is the high frequency contribution, ω_p is the plasma frequency, Γ is the scattering rate. For Al, $\varepsilon_\infty = 1$ F/m, $\omega_p = 1.747 \times 10^{16}$ rad/s, and $\Gamma = 7.596 \times 10^{13}$ rad/s. For N-type Si, it was shown that the Drude model also fit the data well with measurements [30], so here we apply the Drude model with $\varepsilon_\infty = 11.7$ F/m, $\omega_p = 8.92 \times 10^{13}$ rad/s, and $\Gamma = 6.12 \times 10^{13}$ rad/s. The dielectric function of metallic nanoparticle is size-dependent and can be considerably different from that of the bulk material. Although the Drude model is sufficient to describe the optical response of most metals below the threshold for interband electron transitions, it needs to be coupled with interband absorption beyond this threshold. Therefore, the Drude–Lorentz model can be used to describe the dielectric function of metal shell of a core–shell composite nanoparticle,

$$\varepsilon = 1 - \frac{f_0\omega_p^2}{\omega(\omega + i\Gamma_0)} + \sum_j \frac{f_j\omega_p^2}{\omega j^2 - i\omega\Gamma_j - \omega^2} \tag{15}$$

Detailed parameters for metals in Eq. (15) can be referred to [31]. The dielectric function of semiconductor materials can be obtained by the Lorentz model [29]

$$\varepsilon = \varepsilon_\infty\left(1 + \frac{\omega_l{}^2 - \omega_t^2}{\omega_t^2 - \omega^2 - i\Gamma\omega}\right) \tag{16}$$

For SiC, $\varepsilon_\infty = 6.7$ F/m, $\omega_l = 1.827 \times 10^{14}$ rad/s, $\omega_t = 1.495 \times 10^{14}$ rad/s, $\Gamma = 0.9 \times 10^{12}$ rad/s. The dielectric function of core–shell composite nanoparticles can then be obtained by the Maxwell–Garnett approximation method [32]

$$\varepsilon = \varepsilon_1 \frac{\varepsilon_2(1+2f) + \varepsilon_1(1-f)}{\varepsilon_2(1-f) + \varepsilon_1(2+f)} \tag{17}$$

where $f = (r_2^3 - r_1^3)/r_2^3$ is the volume ratio, ε_1 and ε_2 are the dielectric functions of core and shell, respectively.

2.3. Near field radiation

The thermal radiative properties in a plasmonic fluid containing core–shell composite nanoparticles is related to the near field radiation heat flux between the particles. It was demonstrated that collective effects, including hydrodynamics effects due to Brownian motion of nanoparticles and surface plasmon (or phonon-polariton) effect supported by metallic (or polar) nanoparticles, are responsible for the abnormal enhancement of thermal conductivity and hence the heat transfer in a fluid containing nanoparticles [33]. The local thermal fluctuations give rise to oscillations of partial charges which in turn radiate their own electric field in the surrounding medium. In this dimension, strong near field coupling could be predicted when the mean distance between two adjacent nanoparticles in fluid is of the order of their diameter [34,35], suggesting the possibility of a large enhancement of heat transfer from this way. In this investigation, we will estimate the order of magnitude of heat transfer by near field interactions among core–shell composite nanoparticles through modeling the thermal radiative property of two nearest nanoparticle arrays by the fluctuation electrodynamics [7,27]. Since the base medium is usually vacuum in most of the previous researches and the surface resonance is very sensitive to the environment, we also use vacuum for calculation with the fluctuation electrodynamics.

When particle size is smaller than thermal wavelength, near field radiation between two bodies could exceed the blackbody radiation law by several orders of magnitude due to photon tunneling and wave-interference effects. The contribution of fluid molecules to the near field radiation heat flux is negligible comparing with those of nanoparticles, therefore we only consider the near field radiation heat flux between nanoparticle arrays. The near field radiation heat transfer power in unit temperature difference can be obtained by the following relations:

$$P_{ij}^{\mathrm{TE,TM}}(\omega) = \int_0^\infty [P_{\omega\ i->j}^{e,m} - P_{\omega\ j->i}^{e,m}]\mathrm{d}\omega \tag{18}$$

$$P_{\omega i->j}^{e} = \frac{2}{\pi}\frac{\omega^4}{c^4}\mathrm{Im}\alpha_j^e(\omega)\mathrm{Im}\alpha_i^e(\omega)\Theta(\omega,T_i) \times Tr(\boldsymbol{G}(r_j,r_i,\omega)\boldsymbol{G}(r_j,r_i,\omega)) \tag{19}$$

$$P_{\omega i->j}^{m} = \frac{2}{\pi}\frac{\omega^4}{c^4}\mathrm{Im}\alpha_j^m(\omega)\mathrm{Im}\alpha_i^m(\omega)\Theta(\omega,T_i) \times Tr(\boldsymbol{G}(r_j,r_i,\omega)\boldsymbol{G}(r_j,r_i,\omega)) \tag{20}$$

$$\boldsymbol{\alpha}_{i/j}^e(\omega) = 4\pi a_{i/j}^3\left[\frac{\varepsilon_{i/j}-1}{\varepsilon_{i/j}+2} + \frac{1}{12}\left(\frac{\omega a_{i/j}}{c}\right)^2\frac{\varepsilon_{i/j}-1}{\varepsilon_{i/j}+3/2}\right] \tag{21}$$

$$\boldsymbol{\alpha}_{i/j}^m(\omega) = \frac{2\pi}{15}a_{i/j}^3\left(\frac{\omega a_{i/j}}{c}\right)(\varepsilon_{i/j}-1) \tag{22}$$

where P_ω is the monochromatic radiation heat transfer power (radiant heat exchange in unit time and frequency (W/(rad/s)), $\boldsymbol{G}$ is the Green's function, $\boldsymbol{\alpha}_{i/j}^{e/m}$ is the electric/magnetic polarization [19], i and j represent two different nanoparticles, the superscripts TE (or e) and TM (or m) represent the perpendicular and parallel polarizations, respectively. The coupled Green's function in Eqs. (19) and (20) include the specific derivation process which is relatively complex, so the following approximation is used [36]:

$$\sum_{n,m}|G_{nm}(r_j,r_i,\omega)|^2 = \frac{3}{8\pi^2k_0^4|d|^6} \tag{23}$$

where the denominator indicates the heat transfer area, and $k_0 = \omega/c$.

The dipole approximation is used to calculate the near field radiation. This method is valid when the critical vacuum gap d is larger than 4 Å, which corresponds to a transition between the classical and the quantum regions of charge interaction [37]. It has been shown that the dipole approximation takes the major part compared with multiple dipoles when d is larger than the diameter D [38]. At larger separation distances, the multipolar fields become decrease compared with the dipolar ones and the energy of multipolar interactions decreases with the increasing distance d as $O(d^{-(2L+1)})$, where L denotes the multipole order ($L = 1$ for dipole interaction). For two dipoles interaction, the polarization can be simplified as [36]

$$\boldsymbol{\alpha}_{i/j}(\omega) = 4\pi a_{i/j}^3\frac{\varepsilon_{i/j}(\omega)-1}{\varepsilon_{i/j}(\omega)+2} \tag{24}$$

It was shown that the multipolar field can be neglected when calculating the near field heat transfer with higher order term in Eq. (24).

The corresponding radiation heat transfer power (radiant heat exchange in unit time and temperature difference) is

$$P = \int_0^\infty \frac{3\mathrm{Im}\boldsymbol{\alpha}_1(\omega)\mathrm{Im}\alpha_2(\omega)}{4\pi^3d^6}[Q_1(\omega,T) - Q_2(\omega,T)]\mathrm{d}\omega \tag{25}$$

where $Q(\omega,T) = \hbar\omega/2 + \bar{h}\,\omega/(e\hbar^{\omega/(kBT)} - 1)$ is the mean energy of an oscillator, $\hbar = 1.055 \times 10^{-34}$ J s is the reduced Planck constant,

and $k_B = 1.38 \times 10^{-23}$ J/K is the Boltzmann constant. The radiation heat flux between the nanoparticle arrays can be obtained by the Poynting vector S (radiation heat transfer in unit temperature difference) as follows:

$$S = \sum_{i=1}^{N_1} \sum_{j=N_1+1}^{N_1+N_2} (P_{ij}^{TE} + P_{ij}^{TM})/s \tag{26}$$

where s is the radiation heat transfer area of nanoparticles or nanoparticle arrays. The near field radiation is calculated based on the assumptions that the contribution of near field heat transfer in nanocomposites can be divided from thermal interaction between nanoparticle pairs [15,36]. The absence of "collective" effect is due to the rapid decay of the near field radiation heat transfer (d^{-6}) and the reasonably low volume fractions ($f_v = 0.7\%$). We also only consider the longitudinal heat transfer since there is no temperature difference in the same layer. More details will be given in the following section.

3. Results and discussion

3.1. Optical radiative properties

In this numerical calculation, both noble metals (Au and Ag) and base metals (Cu and Al) are simulated to compare for their long-term commercial potential of excellent solar absorption efficient. The outer radii of composite nanoparticles are first set as $r_2 = 5$ nm, and then the outer radius is varied to examine the size effect on the optical radiative properties. In each of the cases, the volume fractions of the composite nanoparticles are set to be $f_v = 0.7\%$ (corresponding to $d = 42$ nm) in order to investigate the absorption and the scattering in the dependent regime.

3.1.1. Absorption efficiency

Defining the particle radius ratio $t = r_1/r_2$, the optical absorption of Si nanoparticle with $r_2 = 5$ nm and that of Si/Au composite nanoparticle with $t = 0.1$, 0.3, 0.5, 0.7 and 0.9 is then calculated, as shown in Fig. 1. It is clear that Si/Au composite nanoparticles exhibit obvious optical absorption enhancement which can be contributed to the LSPR effect excited on the metal surface. As shown in Fig. 1, two resonance peaks can be observed at wavelengths of 0.18 μm and 1.4 μm when $t = 0.9$, for which the shell thickness is small. When increasing the shell thickness with fixed outer radius r_2, the wavelengths of these resonance peaks approach to that at the resonance peak for pure Au nanoparticle, which can be determined as 0.95 μm. It is clear that the optical absorption is enhanced by the severely intensified electric field at resonance wavelength of the Au nanoshell [39], while the shifts of the resonance peaks could be caused by the plasmon hybridization at inner and outer interfaces of the metallic shell nanostructure [40]. It is observed that all the resonance wavelengths at the red-shifted resonance peaks for different radius ratios locate at the range where the solar irradiance is relatively weak, since the visible spectrum is 0.38–0.78 μm. While for the resonance wavelengths at the blue-shifted resonance peaks for different radius ratios, the absorption spectra of the composite nanoparticles will fit the solar spectrum when the radius ratios are smaller than 0.7. Therefore, an excellent solar energy absorber can be produced by using the Si/Au composite nanoparticles which have the LSPR effect excited on the metallic surfaces that can largely enhance the optical absorption. However, an appropriate radius ratio should be determined with consideration of not only the spectra match of absorption and solar irradiance but also the cost of preparation.

The above-mentioned analysis indicates that the absorption efficiency of composite nanoparticles can be obviously influenced by the LSPR effect excited on both surfaces of the metallic material. When the outer radius is varied, the intensity of the LSPR effect at the Au surfaces could be changed, together with the coupling of multi-particles suspended in fluids. Here we still set the volume fraction at 0.7% and fix the radius ratio at 0.3 to observe the variation of absorption efficiency for various outer radius. The results shown in Fig. 2 indicate that the absorption efficiency can be severely intensified at the resonance wavelength, which is 0.5 μm for different outer radius. Both the absorption efficiency and the absorption peaks increase with increasing outer radius. However, there is also no shift of resonance peaks in this case, which indicates that the resonance wavelengths could be shifted when the proportion of the LSPR effect at the metal surfaces is changed, as shown in Fig. 1. Therefore, by appropriate selection of radius ratio of composite nanoparticles with required size and concentration, one can successfully utilize the LSPR effect for efficient solar energy absorption.

3.1.2. Extinction coefficient

It was shown from the above analysis that the nanostructure can dramatically change the optical radiative properties including the extinction coefficient due to its unique absorption and scattering characteristics. For $r_2 = 5$ nm and $f_v = 0.7\%$, the average center-to-center distance between nanoparticles can be determined as $d = 42$ nm, which corresponds to the dependent

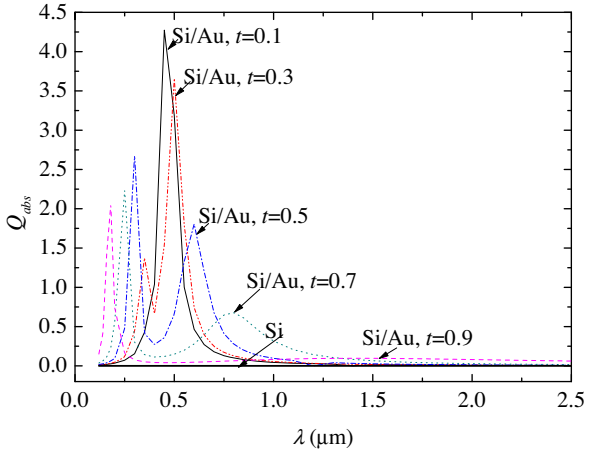

Fig. 1. Absorption efficiency of Si/Au composite nanoparticles with $r_2 = 5$ nm and $f_v = 0.7\%$ ($d = 42$ nm).

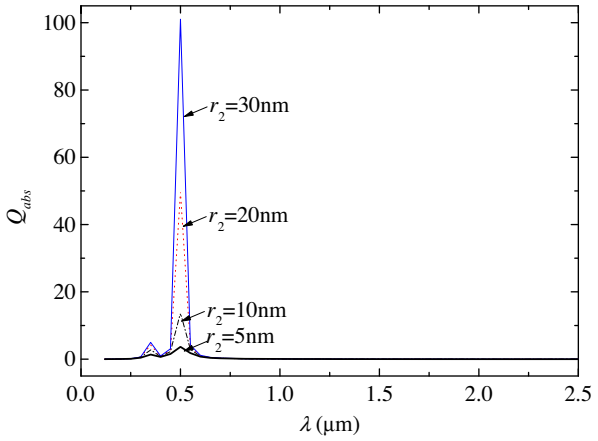

Fig. 2. Absorption efficiency of Si/Au composite nanoparticles with $t = 0.3$ and $f_v = 0.7\%$ ($d = 42$ nm).

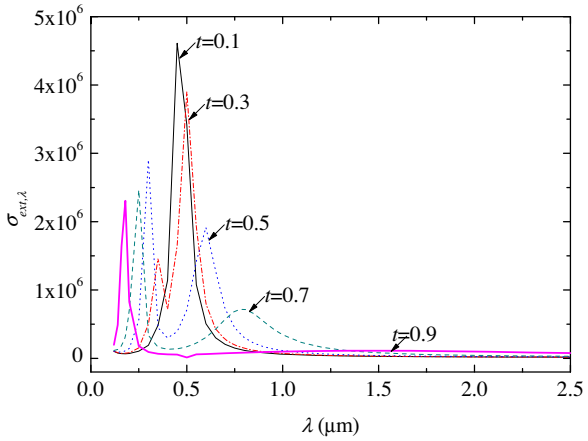

Fig. 3. Extinction coefficients of Si/Au composite nanoparticles with r_2 = 5 nm and f_v = 0.7% (d = 42 nm).

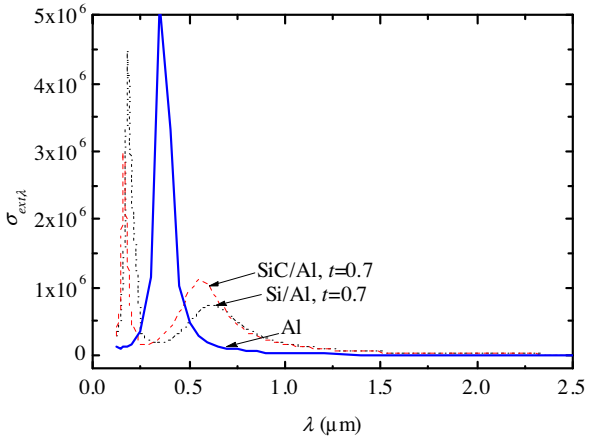

Fig. 5. Extinction coefficient of various nanoparticles of Al surfaces with r_2 = 5 nm and f_v = 0.7% (d = 42 nm).

scattering regime. Increasing the particle radius ratio, the dipole plasmon resonance wavelength, of which the frequency is a function of the radius ratio, will shift to larger wavelengths, creating a red-shift for the maximum extinction coefficients of composite nanoparticles, as shown with the examples of Si/Au core–shell nanoparticles in Fig. 3. Because the solar spectrum range is about 0.25–2.5 μm, which excludes the left peak, here we only consider the contribution of the right peaks or the red shift. When changing the shell thickness at constant particle size, the plasma resonance absorption peak will change obviously – the thinner the shell is, the larger the shift is. This is identical with the analysis of SiO_2/Al composite nanoparticles [41].

To demonstrate the effect of material on extinction coefficient, the extinction coefficients of several core–shell composite nanoparticles with different metallic shells are compared in Fig. 4 when the spectrum range is 0.25–2.5 μm. The result shows that the wavelengths at the maximum extinction coefficient of Si nanoparticle with Al, Cu, Ag and Au shells shift gradually to the long wavelength region. For Ag and Au nanoshells, the maximum extinction coefficients are almost of the same. The maximum extinction coefficient of Cu shell is slightly larger than that of Al shell, and so is Al shell that is larger than Ag or Au shell. Although there exists the shift for these composite nanoparticles, it can be seen from Fig. 4 that Si/Al or Si/Cu core–shell composite nanoparticle would have an equivalent capacity of solar energy absorption as the counterparts with noble metallic nanoshells such as Au and Ag.

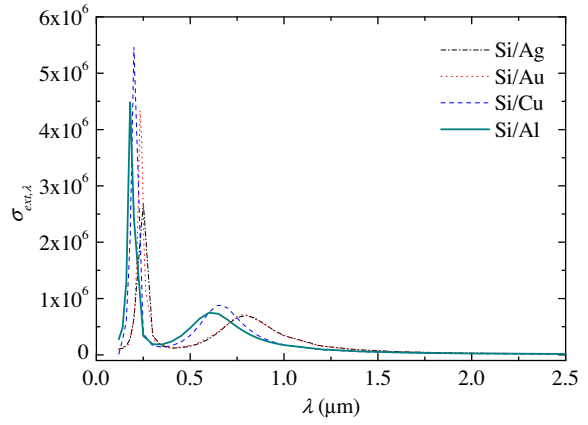

Fig. 4. Extinction coefficient of various composite nanoparticles with r_2 = 5 nm, f_v = 0.7% (d = 42 nm) and t = 0.7.

We further investigate the effect of core material on the extinction coefficient of nanoparticles with Al surfaces, as shown in Fig. 5. It shows that slight difference of extinction coefficient exists among these nanoparticles when the spectrum range is 0.25–2.5 μm. The maximum extinction coefficient of SiC/Al composite nanoparticle is larger than that of Si/Al composite nanoparticle, and the maximum extinction coefficient of Al composite nanoparticle is larger than that of either SiC/Al or Si/Al composite nanoparticle. In general, metal plasma resonance absorption peaks of the composite nanoparticles would have a slight red-shift when comparing with pure metal nanoparticle. In the visible light regime, the maximum extinction coefficients of SiC/Al and Si/Al composite nanoparticles and Al nanoparticles match well with the solar spectrum. Therefore, both SiC/Al, Si/Al and Al nanoparticles are good candidates for efficient solar absorption.

When changing the particle volume fractions, the extinction coefficients of these nanoparticles exhibits quite similar trend except that the amplitudes vary accordingly. For example, the extinction coefficients of the composite nanoparticles at given wavelength are almost twice of the results in Figs. 3–5 when the particle volume fraction is only 0.1% (corresponding to d = 80 nm). This is reasonable since solar irradiance can easily pass through the media in which the average distance between the nanoparticles nearly doubles.

3.1.3. Average radiative thermal conductivity

The energy absorbed by the composite nanoparticles from the excitation can be further radiatively redistributed to the far field or be locally released as heat dissipation due to oscillation damping. Therefore, the average radiative thermal conductivity k_r (W/(m K)) of nanoparticle can be defined to estimate the energy transfer due to absorption or extinction [6],

$$k_r = \frac{16\sigma T^3}{3\sigma_{ext}} \tag{27}$$

where $\sigma = 5.668 \times 10^8$ J/(s m^2 K^4) is the Stefan–Boltzmann constant, T is the temperature, σ_{ext} is the average extinction coefficient of nanoparticles. The average extinction coefficient can be obtained according to the statistics of the total energy attenuation under the temperature T, using the Rosseland approximation formula when the material and the radiation field are in local thermal equilibrium (LTE):

$$1/\sigma_{ext} = \frac{\int_0^\infty \sigma_{ext,\lambda}^{-1}(\partial R_\lambda/\partial T)d\lambda}{\int_0^\infty (\partial R_\lambda/\partial T)d\lambda} \tag{28}$$

Table 1
Average extinction coefficient and radiative thermal conductivity of nanoparticle arrays with $r_2 = 5$ nm, $t = 0.7$ and $f_v = 0.7\%$ ($d = 42$ nm).

Properties	Si/Ag	Si/Au	Si/Cu	Si/Al	SiC/Al	Al
σ_{ext}	19080.46	19354.38	14045.41	16401.73	16158.57	4929.72
k_r (W/(m K))	0.000428	0.000422	0.000581	0.000498	0.000505	0.00166

with the Planck's blackbody radiation intensity R_λ (J/(m Hz)) being defined as

$$R_\lambda = \frac{8\pi hc}{\lambda^5[\exp(hc_0/\lambda k_B T) - 1]} \tag{29}$$

where $h = 6.625 \times 10^{-34}$ J s is the Planck constant, $c_0 = 2.998 \times 10^8$ m/s is the speed of light in vacuum.

Table 1 presents the average extinction coefficient and the average radiative thermal conductivity of different nanoparticles when the ambient temperature $T = 300$ K. It shows that, for composite nanoparticles with metal shells ($r_2 = 5$ nm, $t = 0.7$ and $f_v = 0.7\%$), the minimum and the maximum average extinction coefficients can be obtained when the shell is Cu and Au, respectively; meanwhile, the minimum and the maximum radiative thermal conductivity can be obtained when the shell is Au and Cu, respectively. Both the average extinction coefficient and the radiative thermal conductivity of Si/Al and SiC/Al nanoparticles are close and are in between those of the other composite nanoparticles, especially those of Si/Cu nanoparticle. It also shows that the average extinction coefficients of these composite nanoparticles are all substantially larger than that of the pure Al nanoparticle, although the average radiative thermal conductivities of them are obviously smaller than that of pure nanoparticle.

The average extinction coefficient and the average radiative thermal conductivity increases and decreases with increasing radius ratio, respectively, as shown with the examples of Si/Au, Si/Al and SiC/Al nanoparticles in Table 2. In general, the trend of the optical radiative properties of the composite nanoparticles is the same for both base and noble nanoshells with same thickness. Hence, SiC/Al, Si/Al and Si/Cu composite nanoparticles are perhaps the best candidates for photothermal application in solar collector, if appropriate radius ratio at constant particle volume fraction and radius can be determined to ensure the absorption peak locates at 0.45–0.65 μm.

3.2. Thermal radiative properties

For nanofluid with high volume fraction of nanoparticles, the average distance between adjacent nanoparticles may be small enough such that the near field interaction between nanoparticles should be concerned. In this part, we will estimate the contribution of near field radiation heat flux to the thermal radiative property by two nearest arrays of core–shell composite nanoparticles, which are SiC/Al or Si/Al composite nanoparticles or Al nanoparticles that are promising for application in photothermal conversion, as discussed in the previous subsection. The LSPR effect on nanoscale heat radiation among these nanoparticles is analyzed by the theory of evanescent wave and near field radiation in order to study its impact on related thermal radiative properties, especially the equivalent near field radiative thermal conductivity.

It is noticed that nanofluids may have a spatial distribution for the suspended nanoparticle which can be reasonably described by the log-normal function with respective to the particle radius [42]. However, since most of the particle sizes are close to the average diameter, it is worthwhile investigating the near field radiation heat flux using the average diameter. Meanwhile, we assume here that the nanoparticles are in vacuum condition when calculating the near field radiation heat flux due to the contribution of fluid molecules to it is negligible.

Two 100 × 100 nanoparticle arrays shown in Fig. 6 is chosen for demonstrating the order of magnitude of near field interactions of nanoparticles in fluid. Although it is not practical to find this kind of array in an authentic fluid, it is reasonable to model the heat transfer between two layers with certain temperature difference. The temperature difference is set to be 0.5 K, which is based on the numerical simulation [43]. The near field radiation heat flux between nanoparticle arrays can be obtained by Eq. (26) which is based on the radiation heat transfer between two pure nanoparticles [19]. We set the diameter of the nanoparticles to be 10 nm which has not been investigated much in the literature. The effect of the roughness on the near field heat transfer among nanoparticles, which has been extensively discussed with the proximity approximation (PA) [44] or the Derjaguin approximation [45], is reasonably neglected here.

3.2.1. Monochromatic near field radiation

Near field radiation between two objects can be strongly influenced by changing the temperature or the material. Fig. 7 shows the monochromatic near field radiation power $\boldsymbol{P}_\omega$ between two parallel 100 × 100 Al nanoparticle arrays for different temperature differences and materials when $a = 5$ nm and $d = 11$ nm. Here the relation between $\boldsymbol{P}_\omega$ and the Poynting vector $\overline{\boldsymbol{S}}_\omega$ is $\boldsymbol{P}_\omega = \int \overline{\boldsymbol{S}}_\omega \cdot \boldsymbol{n} \mathrm{d}\sigma = \int \overline{\boldsymbol{S}}_\omega d\sigma$. The results show that, when increasing the temperature difference from 10 K to 50 K, the monochromatic near field radiation power between the Al nanoparticle arrays can be obviously enhanced, with the maximum power for $\Delta T = 50$ K being about six times of that for $\Delta T = 10$ K. However, the monochromatic near field radiation power, especially the maximum power, is obviously deteriorated while employing Au arrays instead of Al arrays when the temperature difference is 10 K. These results clearly indicate that, besides the excellent optical radiative properties and low cost, composite nanoparticles with Al shells can be superior to those with Au shells on the aspect of near field radiation.

The monochromatic near field radiation heat flux between two nanoparticles with $a = 5$ nm, $t = 0.6$ (for composite NPs), $T_1 = 300.5$ K, $T_2 = 300$ K and different center-to-center distances are first given in Fig. 8. Depending on the particle volume fractions which we set as $f_v = 0.1\%$ and 0.7%, the center-to-center distances are determined as $d = 80$ nm and 42 nm, respectively. The temperature difference $\Delta T = 0.5$ K is chosen based on the experiment and simulation in the literature [46]. The result shows that the monochromatic near field radiation heat flux for all cases increases monotonously with the frequency before reaching a maximum value and then decreases monotonously with the frequency. The critical frequency ω_{cr} which corresponds to the maximum monochromatic near field radiation heat flux for a specific nanoparticles does not change. The critical frequencies for Al, SiC/Al and Si/Al nanoparticles are 0.8×10^{14} rad/s, 0.1×10^{15} rad/s and 0.1×10^{14} rad/s, respectively. Meanwhile, the monochromatic near field radiation heat flux at a given frequency decreases with increasing distance for either Al, SiC/Al or Si/Al nanoparticles. Si/Al composite nanoparticles, however, exhibit higher monochromatic near field radiation heat flux at a given frequency comparing with those of other nanoparticles with the same distance or volume fraction.

Fig. 9 presents the variation of monochromatic near field radiation heat flux between two nanoparticles or two parallel 100 × 100 nanoparticle arrays ($N_1 = N_2 = 100$) when $a = 5$ nm, $t = 0.6$ or 0.3 (for composite NPs), $d = 42$ nm, $T_1 = 300.5$ K and $T_2 = 300$ K. When the radius ratio remains at 0.6, the critical frequencies for Al, SiC/Al and Si/Al nanoparticle arrays remain at the values for their nanoparticle counterparts, which are 0.8×10^{14} rad/s, 0.1×10^{15} rad/s and 0.1×10^{14} rad/s, respectively. However, the vertical

Table 2
Average extinction coefficient and radiative thermal conductivity of nanoparticle arrays with r_2 = 5 nm, f_v = 0.7% (d = 42 nm) and different radius ratios.

Properties	Material	t = 0.1	t = 0.3	t = 0.5	t = 0.7	t = 0.9
σ_{ext}	Si/Au	5504.85	6433.30	9135.73	19354.38	68049.06
	Si/Al	5251.12	6047.50	8390.83	16879.17	59826.59
	SiC/Al	5050.88	6039.94	8341.68	16622.45	70950.91
k_r (W/(m K))	Si/Au	0.001483	0.001269	0.000893	0.000422	0.00012
	Si/Al	0.001554	0.001350	0.000973	0.000484	0.000136
	SiC/Al	0.001554	0.001351	0.000978	0.000491	0.000115

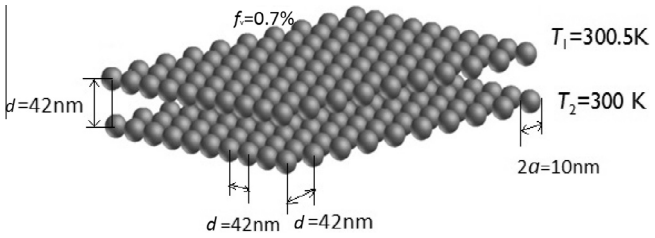

Fig. 6. Two parallel 100 × 100 nanoparticle arrays.

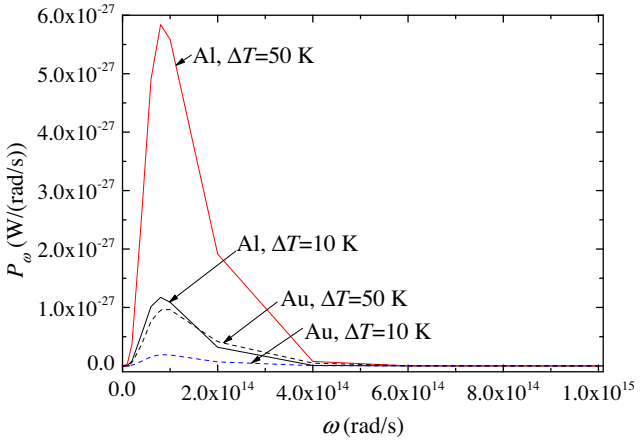

Fig. 7. Monochromatic near field radiation power between two nanoparticle arrays.

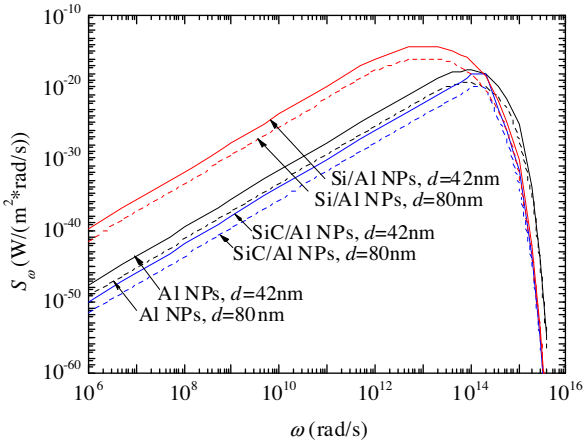

Fig. 8. Monochromatic near field radiation heat flux between two nanoparticles with a = 5 nm, t = 0.6 (for composite NPs), T_1 = 300.5 K, T_2 = 300 K and different center-to-center distances.

monochromatic near field radiation heat flux at a given frequency between the nanoparticle arrays is smaller than that between the nanoparticles due to the larger radiation heat transfer area

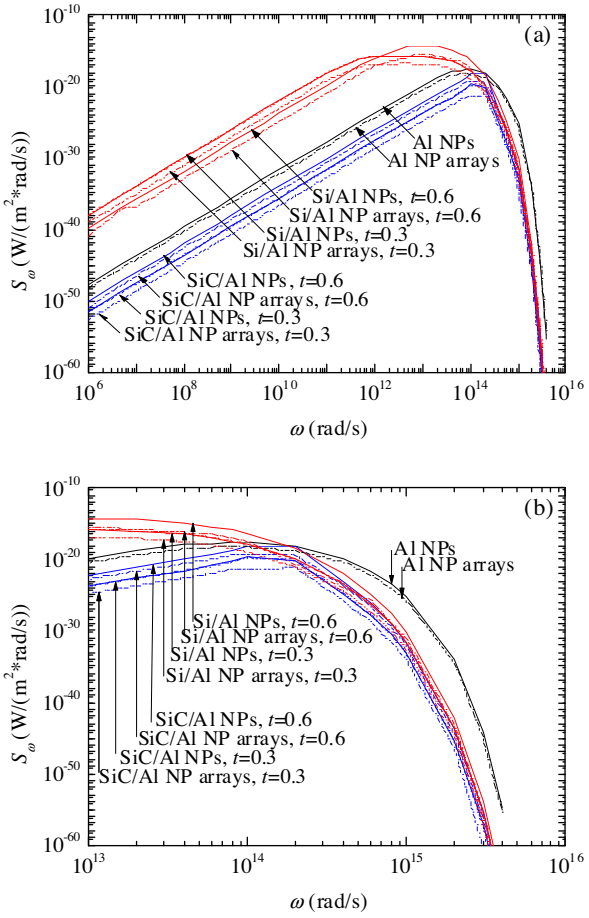

Fig. 9. Monochromatic near field radiation heat flux between two nanoparticles or nanoparticle arrays with a = 5 nm, d = 42 nm, T_1 = 300.5 K and T_2 = 300 K.

($s = \pi(9d + 2a)^2$) for the nanoparticle arrays ($s = \pi a^2$ for the case of nanoparticles, see also Eq. (26)). When the radius ratio varies from 0.6 to 0.3, the critical frequencies for SiC/Al and Si/Al nanoparticles are 0.1×10^{15} rad/s and 0.5×10^{13} rad/s, respectively; while the critical frequencies for SiC/Al and Si/Al nanoparticle arrays are 0.2×10^{15} rad/s and 0.5×10^{13} rad/s, respectively. The frequency shift could be created by the shift of resonant frequency due to the variation of LSPR effects at different radius ratios. It appears that the critical frequency for SiC/Al nanoparticles or nanoparticle arrays tends to shift to larger value, while it tends to shift to smaller value for Si/Al nanoparticles or nanoparticle arrays. The smaller critical frequency for Si/Al nanoparticles or nanoparticle arrays of smaller radius ratio could also lead to the interesting situation that in the low frequency range the monochromatic near field radiation heat flux at a given frequency is higher than the case of higher radius ratio, which is opposite to the cases of SiC/Al and Si/Al in the high frequency range shown in Fig. 9(b). Meanwhile, it generally shows in Fig. 9 that the

Table 3
Near field radiation heat fluxes and effective thermal conductivities of nanoparticles or nanoparticle arrays with $a = 5$ nm, $T_1 = 300.5$ K and $T_2 = 300$ K.

Material	Cases	S (W/m^2)	k_{nf} (W/(m K))
Al	NPs, $d = 80$ nm	0.725×10^{-5}	0.102×10^{-11}
	NPs, $d = 42$ nm	0.346×10^{-3}	0.485×10^{-10}
	NP arrays, $d = 42$ nm	0.923×10^{-4}	0.591×10^{-11}
SiC/Al	NPs, $d = 80$ nm, $t = 0.6$	0.268×10^{-5}	0.375×10^{-12}
	NPs, $d = 42$ nm, $t = 0.6$	0.128×10^{-3}	0.82×10^{-11}
	NPs, $d = 42$ nm, $t = 0.3$	0.272×10^{-5}	0.174×10^{-12}
	NP arrays, $d = 42$ nm, $t = 0.6$	0.117×10^{-4}	0.751×10^{-12}
	NP arrays, $d = 42$ nm, $t = 0.3$	0.153×10^{-6}	0.976×10^{-14}
Si/Al	NPs, $d = 80$ nm	0.35×10^{-2}	0.49×10^{-9}
	NPs, $d = 42$ nm, $t = 0.6$	0.167	0.107×10^{-7}
	NPs, $d = 42$ nm, $t = 0.3$	0.568×10^{-2}	0.364×10^{-9}
	NP arrays, $d = 42$ nm, $t = 0.6$	0.0167	0.107×10^{-8}
	NP arrays, $d = 42$ nm, $t = 0.3$	0.485×10^{-3}	0.31×10^{-10}

Table 4
Effective thermal conductivity of water containing nanoparticles with $a = 5$ nm, $T = 300$ K and Pr = 5.42.

Cases	Si/Ag	Si/Cu	Si/Au	Si/Al	SiC/Al	Al
$d = 80$ nm, $t = 0.6$	0.634	0.637	0.626	0.681	0.674	0.677
$d = 42$ nm, $t = 0.6$	0.731	0.714	0.677	1.058	1.010	1.028
$d = 42$ nm, $t = 0.3$				1.031	1.025	

monochromatic near field radiation heat flux between two Si/Al nanoparticle arrays at a given frequency is the largest among the nanoparticle arrays.

3.2.2. Near field radiative thermal conductivity

Analogous to the definition of thermal conductivity, the average near field radiative thermal conductivity for nanoparticles or nanoparticle arrays can be defined as $k_{nf} = S(d - 2a)/\Delta T$, where the near field radiation heat flux S can be determined by integrating S_ω over ω using Figs. 8 and 9. The calculation of near field radiation heat flux between nanoparticle arrays can be further refined by considering the influence of higher-order multipoles using the dipole approximation method [15]. The results of near field radiation heat fluxes and near field radiative thermal conductivities for Al, SiC/Al and Si/Al nanoparticles or nanoparticle arrays when $a = 5$ nm, $t = 0.6$ or 0.3 (for composite NPs), $d = 42$ nm (for NPs or NP arrays) or 80 nm (for NPs), $T_1 = 300.5$ K and $T_2 = 300$ K are listed in Table 3.

Table 3 indicates that smaller distance results in higher near field radiation heat fluxes for both pure and composite nanoparticles. For nanoparticle arrays, however, the near field radiation heat flux at a given distance is deteriorated by the largely increased heat transfer area when comparing with the case of nanoparticles. Meanwhile, the near field radiation heat fluxes for composite nanoparticles or composite nanoparticle arrays can be obviously reduced by decreasing radius ratio. It is clear that the thickness of metallic nanoshell and hence the LSPR effect interacting at the shell surfaces can substantially vary the near field radiation between two adjacent composite nanoparticles or nanoparticle arrays, of which the distance is kept at constant (here is $d = 42$ nm). It appears that thinner shell create more LSPR at the particle surface and thus enhance the near field radiation between nanoparticles or nanoparticle arrays. However, for $t = 0$ which corresponds to pure metal nanoparticle, the near field radiation heat flux is not the maximum among the calculations. Therefore, there should be an optimal radius ratio that can maximally enhance the near field radiation between nanoparticle arrays.

The variation of near field radiative thermal conductivities over distance, volume fraction (filling fraction) and radius ratio for Al, SiC/Al and Si/Al nanoparticles or nanoparticle arrays, which are also listed in Table 3, exhibit similar trend as that for near field radiation heat fluxes, since k_{nf} is proportional to S according to the definition. The orders of magnitude vary from $O(10^{-14})$–$O(10^{-7})$, from which we can see that material type is the major contributor to this variation. The contributions of the average radiative thermal conductivity and the near field radiative thermal conductivity to the effective thermal conductivity (k_{eff}) of water containing core–shell composite nanoparticles or pure nanoparticles can therefore be evaluated by comparison with the orders of magnitude using the above-calculated results and the calculation of effective thermal conductivity using the extended Maxwell's homogeneous mixing model that considers the effects of nanoparticle [47], including size, surface adsorption, interfacial thermal resistance, clustering and Brownian motion. The effective thermal conductivity of water containing various composite nanoparticles with $a = 5$ nm, $t = 0.6$, $T = 300$ K and Pr = 5.42 is shown in Table 4. The result indicates that the average radiative thermal conductivity and the near field radiative thermal conductivity is far smaller than the effective thermal conductivity of water nanofluids. Therefore, it seems that near field radiation has negligible effect on the heat transfer in nanofluids if the nanoparticles are uniformly distributed. Nevertheless, Si/Al and SiC/Al nanoparticles can be considered as the best candidates for application in efficient photothermal energy conversion.

4. Conclusions

In this paper, we numerically investigated the optical and thermal radiative properties of water-based plasmonic nanofluids containing core–shell composite nanoparticles at given conditions including particle radius ratio, outer radius and type of material. The results show that, by appropriate selection of radius ratio of composite nanoparticles with required size and concentration, one can successfully utilize the LSPR effect for efficient solar energy absorption at the visible and infrared wavelengths. The average extinction coefficient and the average radiative thermal conductivity increases and decreases with increasing radius ratio, respectively, as shown with the examples of Si/Au, Si/Al and SiC/Al nanoparticles. The general trend of the optical radiative properties

of the composite nanoparticles is the same for both base and noble nanoshells with same thickness. Hence, SiC/Al, Si/Al and Si/Cu composite nanoparticles are perhaps the best candidates for photothermal application in solar collector, if appropriate radius ratio at constant particle volume fraction and radius can be determined to ensure the absorption peak locates at 0.45–0.65 μm. Meanwhile, for the optical radiative properties of the composite nanoparticles or nanoparticle arrays, the near field radiation heat fluxes can be obviously reduced by decreasing radius ratio. It appears that thinner shell creates more LSPR at the particle surface and thus enhances the near field radiation between nanoparticles or nanoparticle arrays, but there should be an optimal radius ratio that can maximally enhance the near field radiation between nanoparticle arrays. The results also indicate that the average radiative thermal conductivity and the near field radiative thermal conductivity is far smaller than the effective thermal conductivity of water nanofluids. Therefore, it seems that near field radiation has negligible effect on the heat transfer in nanofluids if the nanoparticles are uniformly distributed. Nevertheless, Si/Al and SiC/Al nanoparticles can be considered as the best candidates for application in efficient photothermal energy conversion.

Conflict of interest

None declared.

Acknowledgments

The authors are grateful to the financial supports by the National Natural Science Foundation of China, the Program for New Century Excellent Talents in University (No. NCET-12-0845), and the Fundamental Research Funds for the Central Universities. The authors also gratefully appreciate the reviewers for their comments.

References

[1] T.P. Otanicar, P.E. Phelan, R.S. Prasher, G. Rosengarten, R.A. Taylor, Nanofluid-based direct absorption solar collector, J. Renewable Sustainable Energy 2 (3) (2010) 033102.
[2] S.U.S. Choi, Enhancing thermal conductivity of fluids with nanoparticles, ASME-Publications-FED 231 (1995) 99–106.
[3] T. Yousefi, E. Shojaeizadeh, F. Veysi, S. Zinadini, An experimental investigation on the effect of pH variation of MWCNT-H_2O nanofluid on the efficiency of a flat-plate solar collector, Sol. Energy 86 (2) (2012) 771–779.
[4] H. Tyagi, P. Phelan, R. Prasher, Predicted efficiency of a low-temperature nanofluid-based direct absorption solar collector, J. Sol. Energy Eng. 131 (4) (2009) 041004.
[5] R. Taylor, S. Coulombe, T. Otanicar, P. Phelan, A. Gunawan, W. Lv, G. Rosengarten, R. Prasher, H. Tyagi, Small particles, big impacts: a review of the diverse applications of nanofluids, J. Appl. Phys. 113 (1) (2013) 011301.
[6] M.F. Modest, Radiative Heat Transfer, third ed., Academic Press, 2013.
[7] Q. Zhu, Z.M. Zhang, Radiative properties of micro-nanoscale particles in dispersions for photothermal energy conversion, in: W.J. Minkowycz, E.M. Sparrow, J.P. Abraham (Eds.), Advances in Numerical Heat Transfer, Nanoparticle Heat Transfer and Fluid Flow, vol. 4, CRC Press/Taylor & Francis, 2012, pp. 143–174.
[8] C. Oubre, P. Nordlander, Optical properties of metallodielectric nanostructures calculated using the finite difference time domain method, J. Phys. Chem. B 108 (46) (2004) 17740–17747.
[9] H. Duan, Y. Xuan, Enhanced optical absorption of the plasmonic nanoshell suspension based on the solar photocatalytic hydrogen production system, Appl. Energy 114 (2014) 22–29.
[10] Y. Xuan, H. Duan, Q. Li, Enhancement of solar energy absorption using a plasmonic nanofluid based on TiO_2/Ag composite nanoparticles, RSC Adv. 4 (31) (2014) 16206–16213.
[11] W. Lv, P.E. Phelan, R. Swaminathan, T.P. Otanicar, R.A. Taylor, Multifunctional core–shell nanoparticle suspensions for efficient absorption, J. Sol. Energy Eng. 135 (2) (2013) 021004.
[12] K. Mallik, M. Mandal, N. Pradhan, T. Pal, Seed mediated formation of bimetallic nanoparticles by UV irradiation: a photochemical approach for the preparation of core–shell type structures, Nano Lett. 1 (6) (2001) 319–322.
[13] R.D. Averitt, D. Sarkar, N.J. Halas, Plasmon resonance shifts of Au-coated Au_2S nanoshells: insight into multicomponent nanoparticle growth, Phys. Rev. Lett. 78 (22) (1997) 4217.
[14] T. Pham, J.B. Jackson, N.J. Halas, T.R. Lee, Preparation and characterization of gold nanoshells coated with self-assembled monolayers, Langmuir 18 (12) (2002) 4915–4920.
[15] S.L. Westcott, S.J. Oldenburg, T.R. Lee, N.J. Halas, Formation and adsorption of clusters of gold nanoparticles onto functionalized silica nanoparticle surfaces, Langmuir 14 (19) (1998) 5396–5401.
[16] C.-L. Tien, B.L. Drolen, Thermal radiation in particulate media with dependent and independent scattering, Annu. Rev. Heat Transfer 1 (1) (1987) 1–32.
[17] S. Volz, G. Domingues, Near-field heat transfer percolation in nanoparticles based composite media, J. Nanoelectron. Optoelectron. 1 (2006) 224.
[18] J.Y. Lu, Y.H. Chang, Implementation of an efficient dielectric function into the finite difference time domain method for simulating the coupling between localized surface plasmons of nanostructures, Superlattices Microstruct. 47 (1) (2010) 60–65.
[19] A.D. Phan, L.M. Woods, Near-field heat transfer between gold nanoparticle arrays, J. Appl. Phys. 114 (21) (2013) 214306.
[20] E. Petryayeva, U.J. Krull, Localized surface plasmon resonance: nanostructures, bioassays and biosensing – a review, Anal. Chim. Acta 706 (1) (2011) 8–24.
[21] K.L. Kelly, E. Coronado, L.L. Zhao, G.C. Schatz, The optical properties of metal nanoparticles: the influence of size, shape, dielectric environment, J. Phys. Chem. B 107 (3) (2003) 668–677.
[22] T.R. Jensen, M.D. Malinsky, C.L. Haynes, R.P. Van Duyne, Nanosphere lithography: tunable localized surface plasmon resonance spectra of silver nanoparticles, J. Phys. Chem. B 104 (45) (2000) 10549–10556.
[23] R.A. Taylor, P.E. Phelan, T.P. Otanicar, R. Adrian, R. Prasher, Nanofluid optical property characterization: towards efficient direct absorption solar collectors, Nanoscale Res. Lett. 6 (1) (2011) 1–11.
[24] B. Lim, H. Kobayashi, T. Yu, J. Wang, M.J. Kim, Z.-Y. Li, M. Rycenga, Y. Xia, Synthesis of Pd–Au bimetallic nanocrystals via controlled overgrowth, J. Am. Chem. Soc. 132 (8) (2010) 2506–2507.
[25] B.L. Drolen, C.L. Tien, Independent and dependent scattering in packed-sphere systems, J. Thermophys. Heat Transfer 1 (1) (1987) 63–68.
[26] J.D. Cartigny, Y. Yamada, C.L. Tien, Radiative transfer with dependent scattering by particles: Part 1 – Theoretical investigation, ASME J. Heat Transfer 108 (3) (1986) 608–613.
[27] A.I. Volokitin, B.N.J. Persson, Radiative heat transfer between nanostructures, Phys. Rev. B 63 (20) (2001) 205404.
[28] V. Twerskyt, Transparency of pair-correlated, random distributions of small scatterers, with applications to the cornea, J. Opt. Soc. Am. 65 (5) (1975) 524–530.
[29] Z.M. Zhang, Nano/Microscale Heat Transfer, McGraw-Hill, 2007.
[30] E.D. Palik, Handbook of Optical Constants of Solids, Academic Press, 1985.
[31] A.D. Rakic, A.B. Djurišic, J.M. Elazar, M.L. Majewski, Optical properties of metallic films for vertical-cavity optoelectronic devices, Appl. Opt. 37 (22) (1998) 5271–5283.
[32] G. Maxwell, Colours in metal glasses and metal films, Philos. Trans. R. Soc. Lond. A 3 (1904) 385–420.
[33] M. Vladkov, J.-L. Barrat, Modeling thermal conductivity and collective effects in a simple nanofluid, J. Comput. Theor. Nanosci. 5 (2) (2008) 187–193.
[34] A.I. Volokitin, B.N.J. Persson, Resonant photon tunneling enhancement of the radiative heat transfer, Phys. Rev. B 69 (4) (2004) 045417.
[35] G. Domingues, S. Volz, K. Joulain, J.-J. Greffet, Heat transfer between two nanoparticles through near field interaction, Phys. Rev. Lett. 94 (8) (2005) 085901.
[36] K. Joulain, J.-P. Mulet, F. Marquier, R. Carminati, J.-J. Greffet, Surface electromagnetic waves thermally excited: Radiative heat transfer, coherence properties and Casimir forces revisited in the near field, Surf. Sci. Rep. 57 (3) (2005) 59–112.
[37] S. Xiong, K. Yang, Y.A. Kosevich, Y. Chalopin, R. D'Agosta, P. Cortona, S. Volz, Classical to quantum transition of heat transfer between two silica clusters, Phys. Rev. Lett. 112 (11) (2014) 114301.
[38] P. Ben-Abdallah, R. Messina, S.-A. Biehs, M. Tschikin, K. Joulain, C. Henkel, Heat superdiffusion in plasmonic nanostructure networks, Phys. Rev. Lett. 111 (17) (2013) 174301.
[39] V.E. Ferry, A. Polman, H.A. Atwater, Modeling light trapping in nanostructured solar cells, ACS Nano 5 (12) (2011) 10055–10064.
[40] E. Prodan, P.J.C.P. Nordlander, Plasmon hybridization in spherical nanoparticles, J. Chem. Phys. 120 (11) (2004) 5444–5454.
[41] S.J. Oldenburg, R.D. Averitt, S.L. Westcott, N.J. Halas, Nanoengineering of optical resonances, Chem. Phys. Lett. 288 (2) (1998) 243–247.
[42] B.-X. Wang, L.-P. Zhou, X.-F. Peng, A fractal model for predicting the effective thermal conductivity of liquid with suspension of nanoparticles, Int. J. Heat Mass Transfer 46 (14) (2003) 2665–2672.
[43] A. Lenert, E.N. Wang, Optimization of nanofluid volumetric receivers for solar thermal energy conversion, Sol. Energy 86 (1) (2012) 253–265.
[44] B.N. Persson, B. Lorenz, A.I. Volokitin, Heat transfer between elastic solids with randomly rough surfaces, Eur. Phys. J. E 31 (1) (2010) 3–24.
[45] S.-A. Biehs, J.-J. Greffet, Influence of roughness on near-field heat transfer between two plates, Phys. Rev. B 82 (24) (2010) 245410.
[46] A. Veeraragavan, A. Lenert, B. Yilbas, S. Al-Dini, E.N. Wang, Analytical model for the design of volumetric solar flow receivers, Int. J. Heat Mass Transfer 55 (4) (2012) 556–564.
[47] J.-J. Zhao, Y.-Y. Duan, X.-D. Wang, B.-X. Wang, Effect of nanofluids on thin film evaporation in microchannels, J. Nanopart. Res. 13 (10) (2011) 5033–5047.